Ordered Mesoporous Carbons with Various Pore Sizes: Preparation and Naphthalene Adsorption Performance

Keliang Wang,[1,2] Bichun Huang,[1,3] Dongmei Liu,[1] Daiqi Ye[1,3]

[1]*College of Environmental Science and Engineering, South China University of Technology, Guangzhou 510006, China*
[2]*College of Science, Xi'an University of Architecture and Technology, Xi'an 710055, China*
[3]*Key Lab of Pollution Control and Ecosystem Restoration in Industry Clusters (South China University of Technology), Ministry of Education, Guangzhou 510006, China*

Received 8 October 2010; accepted 25 September 2011
DOI 10.1002/app.36382
Published online in Wiley Online Library (wileyonlinelibrary.com).

ABSTRACT: Ordered mesoporous carbons (OMCs) with tunable pores were synthesized by a soft-template method with F127 as a template and boric acid as a pore regulator agent. The prepared samples were characterized by small-angle X-ray diffraction, transmission electron microscopy, Fourier transform infrared spectroscopy, and N_2 adsorption–desorption. The results show that the OMCs had well ordered, two-dimensional (2D) hexagonal structures and the pore sizes were finely tunable in the range 3.4–4.7 nm when boric acid was used as the pore regulator agent. The adsorption experiments showed that the OMCs had a strong adsorption affinity to naphthalene and the maximum adsorption amount was shown to reach up to 303.2 mg/g. Furthermore, the mesopore volume between 2 and 3.5 nm of OMCs was crucial to the adsorption capacity, and OMCs with pore sizes of 2–3.5 nm were much more favorable for the naphthalene adsorption process. The adsorption isotherms of naphthalene on OMCs matched well with the Langmuir adsorption isotherm. Theoretical studies showed that the adsorption kinetics of naphthalene on OMCs accounted well for the use of the Langmuir adsorption kinetics equation. © 2012 Wiley Periodicals, Inc. J Appl Polym Sci 000: 000–000, 2012

Key words: adsorption; templates; TEM

INTRODUCTION

Polycyclic aromatic hydrocarbons (PAHs) are a large group of organic compounds with two or more fused aromatic rings. As environmental pollutants, they are of concern because some compounds are able to change the normal metabolic functions of cells and produce mutagenic, carcinogenic, and teratologic effects.[1–3] They are formed mainly by pyrolytic processes, including the incomplete combustion of carbon-containing materials (e.g., wood, coal, crude oil, natural gas), vehicle traffic, cooking or tobacco smoke, and other human activities. Because of their high volatility and reactivity,[4] PAHs are not only adsorbed on the surface of particulate matter but also suspended in the gas phase.[5,6] Accordingly, adsorption is a practical way to remove PAHs.[7–9]

Porous carbon materials (e.g., active carbon, carbon molecular sieves, active carbon fibers) have been used widely as adsorbants in air pollution control. Mastral et al.[10] reported that 16 carbon materials were used to study the adsorption capacities of naphthalene, phenanthrene, and pyrene. They concluded that the higher micropore volumes of the carbon materials were, the higher the adsorption capacities were. Additionally, the PAH adsorption capacity was directly related to the micropore size, micropore distribution, and mesopore volume.

Micropores (pore diameter $\leq$ 2 nm), which make up a high proportion of active carbon materials, prohibit some macromolecules or compounds access and result in a low adsorption capacity.[11] However, in recent years, mesoporous (pore diameter = 2–50 nm) carbon materials[12] have been found to be interest because of their high surface areas, large pore volumes, and uniform pore sizes. Xu et al.[13] synthesized mesoporous carbons with high surface areas and large pore volumes using mesophase pitch as a carbon precursor and nanosized MgO as an additive. Their research indicated that the adsorption of commercial active carbons to vitamin B12 was lower than that of mesoporous carbons. Yan et al.[14] developed a vapor-deposition polymerization method for the preparation of mesoporous carbons by using acid- and alkaline-treated zeolite X as the template and furfuryl alcohol as the carbon source. They found that the equilibrium adsorption capacity (Q_e) of methylene blue onto the prepared carbons could reach 380 mg/g, and the adsorption kinetics could be well depicted with a pseudo-second-order kinetic model. However, the

Correspondence to: B. Huang (cebhuang@scut.edu.cn).
Contract grant sponsor: China's Ministry of Science and Technology under the National High Technology Development "863" Plan; contract grant number: 2006AA06A310.
Contract grant sponsor: Scientific and Technological Project of Guangdong Province; contract grant number: 2008B050100007 and 2009B050900005.

influence of mesoporous structures on the adsorption property still needs further research. In summary, these mesoporous carbon materials have various mesoporous structures but are not favored for researching the adsorption mechanism because their pore channel arrangement is disordered and their pore size distribution is wide.

Ordered mesoporous carbons (OMCs), which are synthesized with amphoteric surfactants as a template, can offer great potential for use in various applications, such as catalyst supports for fuel cells, carbon electrodes for supercapacitors, chromatography separation, hydrogen storage/conversion devices, adsorption to large molecules, and desulfurization for clean energy.[15–22] This is due to their well-ordered pore structures, regulated pore size, large pore volume, high specific surface area, and narrow pore size distribution. There have been many articles reporting the preparation and adsorption properties of OMCs in the liquid phase.[23–26] However, until now, the adsorption of PAHs in the gas phase has rarely been reported.[27–30]

In this study, OMCs were synthesized by a soft-template method, and the pore sizes were regulated with boric acid as a pore regulator. The textual structures of the OMCs were investigated by small-angle X-ray diffraction (XRD), transmission electron microscopy (TEM), Fourier transform infrared (FTIR) spectroscopy, and N_2 adsorption. The adsorption isotherms and kinetics of naphthalene on the OMCs were also investigated with the Langmuir model in a fixed bed. The OMCs exhibited a high surface area and large adsorption amounts of naphthalene, and their mesoporocity probably played a key role in their adsorption capacity. These results may provide some useful information for further research on the preparation of OMCs and the removal of PAHs.

EXPERIMENTAL

Reagents and materials

The triblock copolymer pluronic F127 (weight-average molecular weight = 12,600, Poly(ethylene oxide)$_{106}$-poly(propylene oxide)$_{70}$-poly(ethylene oxide)$_{106}$ (PEO_{106}–PPO_{70}–PEO_{106}) was purchased from Sigma-Aldrich (St Louis, MO, USA). NaOH, hydrofluoric acid, boric acid, absolute ethyl alcohol, phenol, formaldehyde (37 wt %), and HCl (36 wt %) were provided by the Guangzhou Chemical Reagent Factory (Guangzhou, China). All of these materials were used without further purification. Deionized water was used throughout this work.

Preparation of resol precursor

OMCs were prepared with F127 as the template and phenol–formaldehyde resin (PF resin) as the carbon precursor. The molar ratios of the synthesis compositions were phenol/formaldehyde/NaOH/F127/boric acid = 1 : 2 : 0.1 : 0.015 : 0–0.9. The OMCs were denoted as OMC-Bx, where the x (the molar percentage of boric acid to phenol) values were 0, 10, 50, and 90. The soluble phenolic resin was prepared from phenol and formaldehyde according to procedures reported elsewhere.[31,32] Typically, 2.49 g of phenol was melted at 40°C; this was followed by stirring with 1.3 mL of a 2 mol/L NaOH aqueous solution for 10 min. Then, 3.8 mL of a formaldehyde aqueous solution (37.0 wt %) was added dropwise at 50°C. After further stirring for 1 h at 70°C, the mixture was cooled to room temperature. The pH value was adjusted to 7.0 with a 0.6 mol/L HCl solution. Water was removed by vacuum distillation below 50°C. The final product was dissolved in ethanol to remove the NaCl precipitates; this yielded a 20 wt % resol solution.

Preparation of the OMCs

A typical synthetic mesoporous carbon process is described[31–34] as follows: 5 g of F127 and boric acid were dissolved in 40 mL of ethanol, and then, 25.0 g of 20 wt % PF resin ethanol solution was added with stirring for 20 min at room temperature. So a gluelike mixture was formed after the partial ethanol was evaporated. Afterward, the mixture was dried at 100°C for 24 h and then at 160°C for 6 h. The obtained solid product was ground into a powder and transferred to a quartz boat. The calcination was carried out in a tubular furnace at 450°C for 2 h and at 900°C for 3 h under an N_2 flow. The heating rate was 1°C/min below 450 and 5°C/min above 450°C. This was followed by leaching with an aqueous HF (10.0 wt %) solution for 24 h to remove the template. Finally, the well-OMCs were obtained after filtration, washing, and drying.

Material characterization

FTIR spectroscopy was used to investigate the bonding structure of the OMCs. FTIR spectra of samples were collected on an EQUINOX55 spectrometer (Bruker, Ettlingen, Germany) in the wave-number range 500–4000 cm^{-1} with a resolution of 4 cm^{-1} at room temperature. XRD measurements were taken on a D8 Advance diffractometer (Bruker) with Ni-filtered Cu Kα radiation (λ = 0.15418 nm, 40 kV, 40 mA) in the 2θ range 0.6–6°. The morphologies of the OMCs were observed under TEM, and TEM experiments were conducted with a JEM-2010HR microscope (JEOL, Tokyo, Japan) operated at 200 kV. The nitrogen adsorption–desorption isotherms of the OMCs were measured on an ASAP2010 (Micromeritics, Norcross, GA, USA). The measurements were

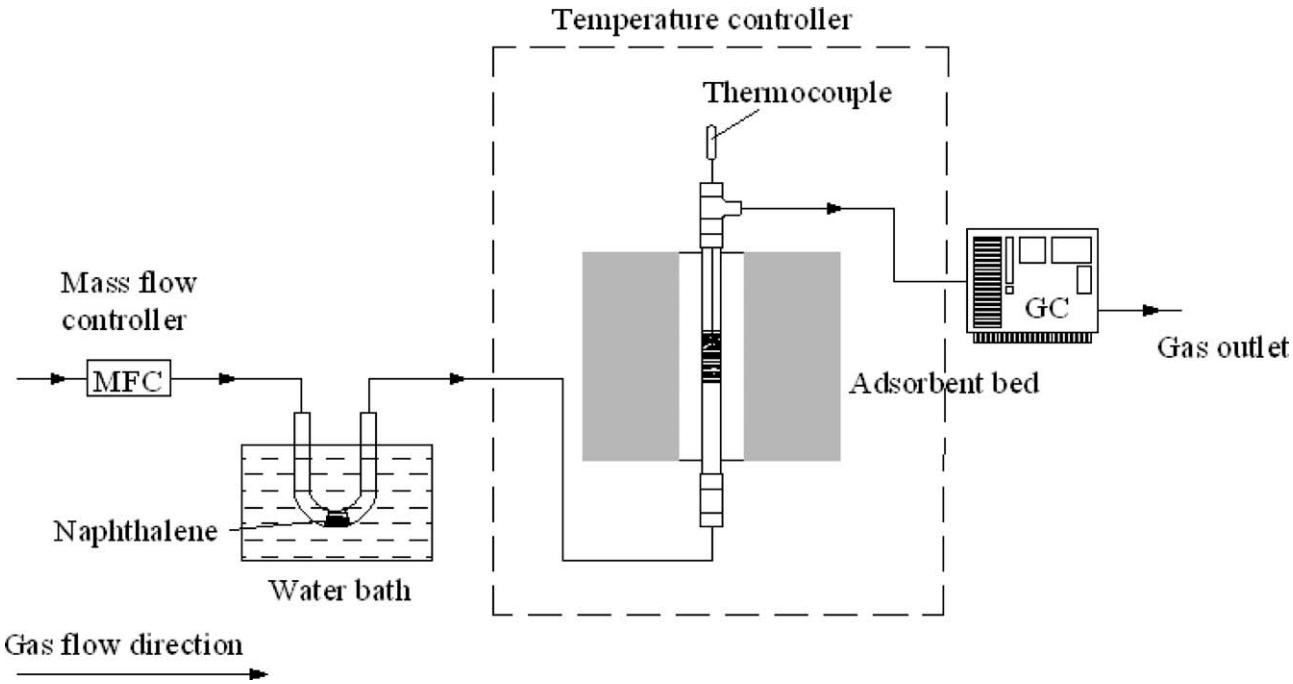

Figure 1 Specific experimental setup for naphthalene adsorption.

performed at 77 K (liquid nitrogen temperature) with a static volumetric method. The Brunauer–Emmett–Teller (BET) method was used to calculate the specific surface areas (S_{BET}) with the adsorption data in relative pressure ranges from 0.04 to 0.2. With the Barrett–Joyner–Halenda (BJH) model,[35] the pore volume and pore size distribution were derived from the adsorption branches of isotherms, and the total pore volumes were estimated from the adsorbed amounts at a relative pressure (P/P_0) of 0.98.

Naphthalene adsorption on OMCs

Naphthalene adsorption experiments were carried out with a laboratory-scaled apparatus, and the schematic of the apparatus is shown in Figure 1. The adsorption reactor was made of quartz glass with an outer diameter of 10 mm, an effective length of 500 mm, and a thickness of 1 mm. The reactor, composed of 100.0 mg of adsorbent (OMCs), was mixed with 0.6 g of quartz sand to provide enough bed length (24 mm); we assessed, in this way, a uniform flow throughout the reactor. During the experiments, the superficial gas flow rate was 3.32 cm/s, and the residence time was 0.72 s.

The naphthalene was sublimated in the U-tube, and the inlet stream concentration of naphthalene was adjusted by changes in the temperature of the water bath. This was then sent into the adsorption reactor with flowing dry air. The naphthalene inlet and outlet stream concentrations were analyzed online with a gas chromatograph (Techcomp, GC7890, Shanghai, China).

The adsorption capacity of naphthalene on the OMCs was determined with the following equation:

$$Q_e = \frac{(C_0 t - S)u}{M_{\mathrm{OMCs}}} \quad (1)$$

where Q_e is the equilibrium adsorption capacity (mg/g), C_0 is the naphthalene inlet stream concentration (mg/mL), t is the equilibrium adsorption time (min; t was measured when the outlet stream concentration of naphthalene reached 90% of the inlet stream concentration of naphthalene), S is the area surrounded by the breakthrough curve and contact time in Figure 6 (m^2; figure is shown later;), u is the flow rate (mL/min), and M_{OMCs} is the adsorbent weight (g).

RESULTS AND DISCUSSION

Characterization of the OMCs

FTIR spectroscopy

The FTIR spectra of the OMC-Bx samples after calcination are shown in Figure 2. The results show that the bands at 2920 and 1090 cm^{-1} were attributed to the C—H and C—O stretching of the triblock copolymer F127.[36] A broad band at 3440 cm^{-1} was associated with the —OH stretching and suggested the existence of a phenolic—OH group. The weak bands at 1640 and 1561 cm^{-1} were assigned to C—C stretching vibration of phenolic resins.[37,38] The spectra of the samples did not change significantly during calcination and the addition of boric acid; this indicated

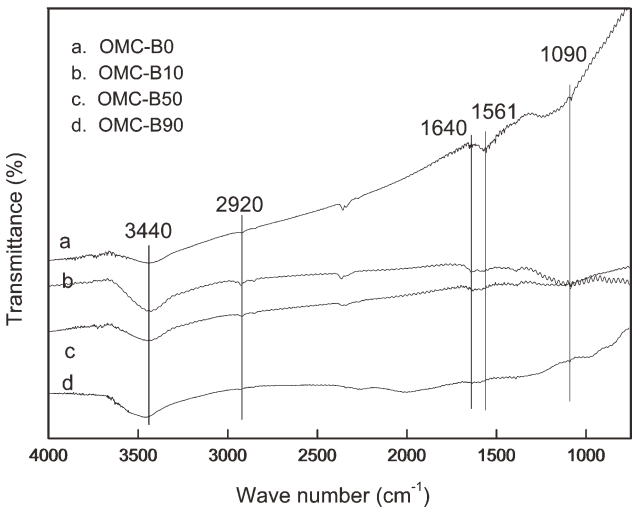

Figure 2 FTIR spectra of the OMCs.

that boron oxide was removed by leaching with HF solution. For the OMC-B*x* samples, the FTIR spectra showed weak intensity, and the intensity was similar at different bands. This proved that Pluronic F127 was almost completely eliminated, and the phenolic resins were almost entirely carbonized. Also, the FTIR spectra of mesoporous carbon clearly indicated the framework was composed of carbon.

Small-angle XRD

The small-angle XRD patterns of OMC-B*x* are illustrated in Figure 3. The OMC-B0 revealed three well-resolved peaks, which were indexed to the (100), (110), and (200) diffraction peaks of a space group P6mm hexagonal structure.[39] The values of interplanar spacing (*d*) were 8.8, 5.1, and 4.4 nm, respectively. Their ratios corresponded to $1:(1/\sqrt{3}):(1/2)$, which indicated that the OMCs had well-ordered 2D hexagonal structures. However, the higher boric acid content led to structural changes, as revealed by a slight shift to lower 2θ angles and a sharper (100) peak XRD reflections. For OMC-B0, OMC-B10, OMC-B50, and OMC-B90, the unit cell size ($a_0 = 2d_{100}/\sqrt{3}$) values were 12.1, 10.9, 10.3, and 10.1 nm, respectively. Combined with the most probable pore diameter of OMC-B*x* (in Table I), this indicated that the pore walls became thinner.[40] In addition, the low-angle XRD peaks in the patterns of OMC-B*x* were significantly higher in intensity, and the value of *d* increased with the higher content of boric acid. This suggested that the shrinkage extent of the framework was lower during carbonization, whereas the pore sizes increased.

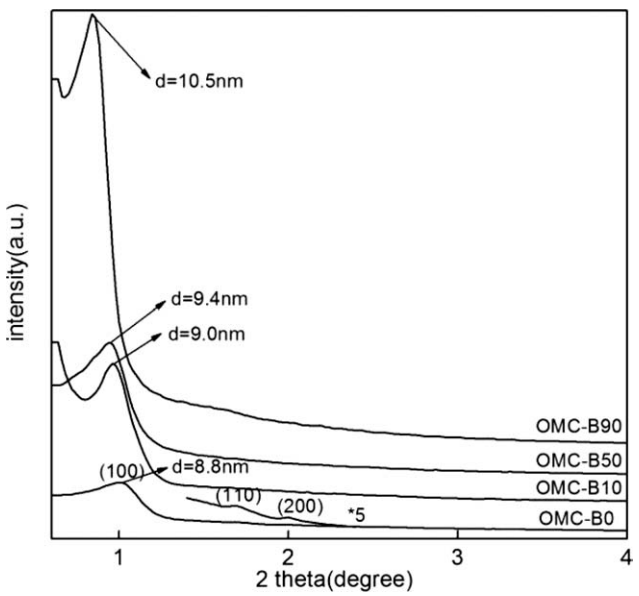

Figure 3 Small-angle XRD patterns of the OMCs (*5, 5× vertical increase for OMC-B0).

TABLE I
Physical Properties of the OMCs

Sample	D_{BJH} (nm)	S_{BET} (m^2/g)	V_{total} (cm^3/g)	V_{meso} (cm^3/g)	$V_{2–3.5nm}$ (cm^3/g)
OMC-B0	3.4	505	0.34	0.23	0.12
OMC-B10	3.5	611	0.37	0.20	0.16
OMC-B50	4.0	558	0.39	0.26	0.11
OMC-B90	4.7	680	0.58	0.47	0.08

D_{BJH}, pore size; S_{BET}, BET surface area; V_{total}, total pore volume at $P/P_0 = 0.98$; V_{meso}, mesopore volume; $V_{2–3.5nm}$, mesopore volume between 2 and 3.5 nm.

TEM

The high-resolution TEM images of OMC-B0 showed a highly ordered degree of periodicity, viewed along the (100) and (110) directions (A and B in Fig. 4); this further confirmed the 2D hexagonal P6mm arrangement of pores with uniform sizes and well-aligned channels. The pore diameters of OMC-B0, OMC-B10, OMC-B50, and OMC-B90, estimated from the TEM images, were 3.7, 3.8, 4.2, and 5.0 nm, respectively. These values were consistent with the nitrogen adsorption results (Table I). For the other three samples (OMC-B10, OMC-B50, and OMC-B90) with different boric acid amounts, the order of mesoporous structure was preserved (C, D, E, F, G, and H in Fig. 4). This indicated that the addition of boric acid did not destroy the highly ordered structure. In addition, no other mesophase could be observed; this implied that the ordered 2D hexagonal mesostructure was a pure phase, and the OMC-B*x* had well-ordered hexagonal arrays with 1D channels, even after calcination at 900°C. This indicated a high thermal stability.

Nitrogen adsorption isotherms and pore sizes distribution of the OMCs

Figure 5(A) presents the nitrogen adsorption isotherms of the OMCs. The observed steep adsorption

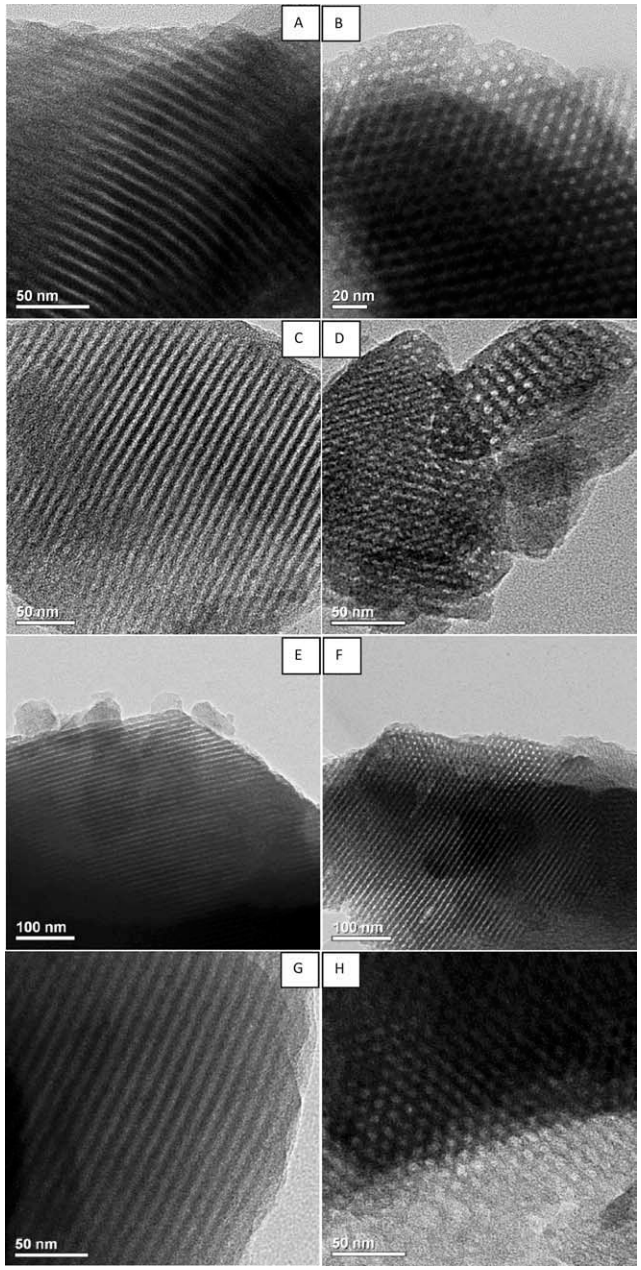

Figure 4 TEM images of (A,B) OMC-B0, (C,D) OMC-10, (E,F) OMC-B50, and (G,H) OMC-B90 viewed along the (A,C,E,G) (100) and (B,D,F,H) (110) directions

increase in the OMCs at 77 K was of type Langmuir IV with a clear H1-type hysteresis loop for relative pressures from 0.4 to 0.8. This is characteristic of highly ordered mesoporous materials. The pore size distributions are shown in Figure 5(B). The values were 3.4 nm (OMC-B0), 3.5 nm (OMC-B10), 4.0 nm (OMC-B50), and 4.7 nm (OMC-B90), respectively. The mesopores were concentrated in a relatively small size range. Quantitative analysis of the OMCs showed that the most probable pore diameter of the OMCs was larger with increasing boric acid content. The detailed textural data of the samples are provided in Table I, which shows that not only the pore sizes but also the surface area increased with the addition of boric acid to the OMCs. However, this was not a significantly positive correlation. Additionally, the total pore volume and mesopore volume also increased with the added boric acid amount, except for the sample OMC-B10. This corresponded with the hysteresis loop size of the nitrogen adsorption isotherms, as shown in Figure 5(A).

Breakthrough curves of naphthalene on the OMCs

The adsorption of naphthalene on the OMCs was examined under the following experimental conditions: an adsorption temperature of 150°C and an initial naphthalene concentration of 0.00126 mg/mL. The breakthrough curves (Fig. 6) showed that the breakthrough time for OMC-B10 was longer than those of the other three samples, and the order was OMC-B10 > OMC-B0 > OMC-B50 > OMC-B90. The adsorbed amounts of naphthalene for OMCs could be calculated with eq. (1), and the results are as follows: OMC-B10 (303.2 mg/g) > OMC-B0 (245.9 mg/g) > OMC-B50 (205.5 mg/g) > OMC-B90 (126.3 mg/g). The OMC-B90 sample had the shortest equilibrium adsorption time, and its mesopore volume was the largest (Table I). The results demonstrate that increasing the mesopore volume shortened the time to reach equilibrium adsorption. The surface functional groups of the OMCs did not change, as shown in Figure 2. Additionally, the naphthalene adsorption amount for OMC-B90 was the lowest, even though it had the largest surface area (Table I). In summary, a conclusion could be drawn that the surface functional groups hardly affected the adsorption capacity of naphthalene, and there were no correlations between the surface area of the OMCs and the adsorption capacity.

On the basis of the results in Table I, the mesopore volume and the most probable pore diameter of OMC-B10 were smaller than those of the other three samples. Also, the mesopore volume between 2 and 3.5 nm of the OMCs followed the step-down order of OMC-B10 > OMC-B0 > OMC-B50 > OMC-B90. This was coincident with the order of adsorption amount of naphthalene [Fig. 7(a–c). The result also revealed that the pore sizes (2–3.5 nm) were very important for the adsorption process.

Adsorption isotherms of naphthalene on OMCs

The adsorption isotherms indicated the partition of adsorbate between gas and adsorbent at equilibrium. The Langmuir isotherm is used most widely[41] and is suitable for describing monocomponent adsorption. In this study, the adsorption isotherms of naphthalene on the OMCs were investigated at 120, 150, and

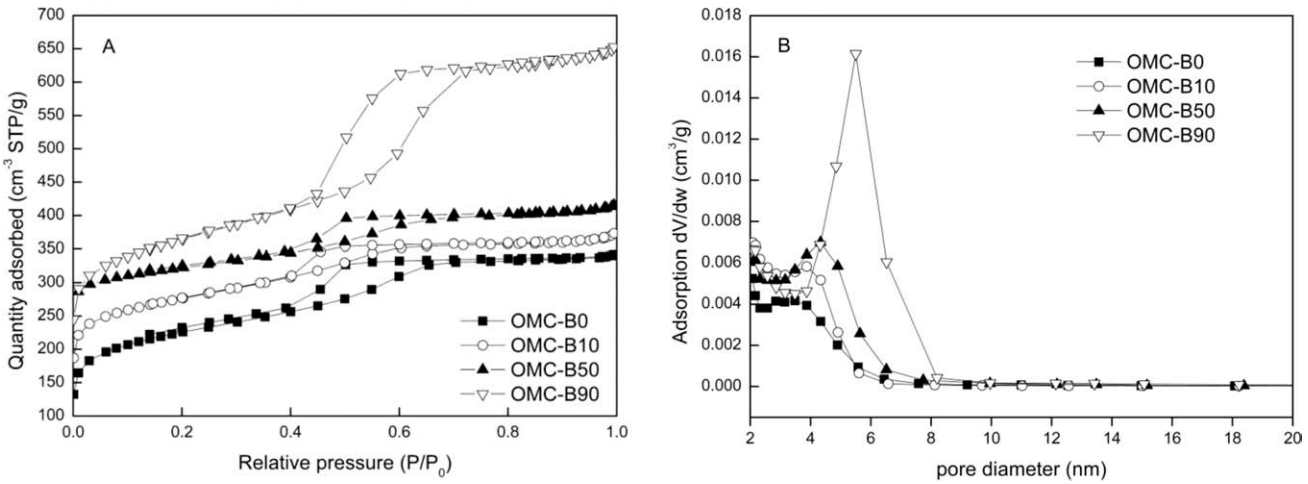

Figure 5 (A) Nitrogen adsorption–desorption isotherms and (B) pore size distribution of the OMCs. The isotherms for OMC-B50 and OMC-B90 were offset vertically by 160 and 60 cm^3/g, respectively

180°C, respectively. The adsorption data fit the Langmuir isotherm. The results are shown in Figure 7 and Table II.

The Langmuir equation is as follows:[42]

$$q_e = \frac{Q_0 b C_e}{1 + bC_e} \tag{2}$$

where q_e and Q_0 are the equilibrium and maximum adsorption capacities (mg/g), respectively, C_e is the equilibrium concentration (mg/mL), and b is the equilibrium constant (mL/mg).

The data shown in Figure 7 indicated that the equilibrium capacities for all samples increased with higher naphthalene equilibrium concentrations. However, the rate of the increase was different. Meanwhile, the data also suggest that the equilibrium capacities decreased with increasing temperature. The results indicate that naphthalene adsorption on the OMCs was an exothermic process, which is a typical characteristic of physical adsorption.

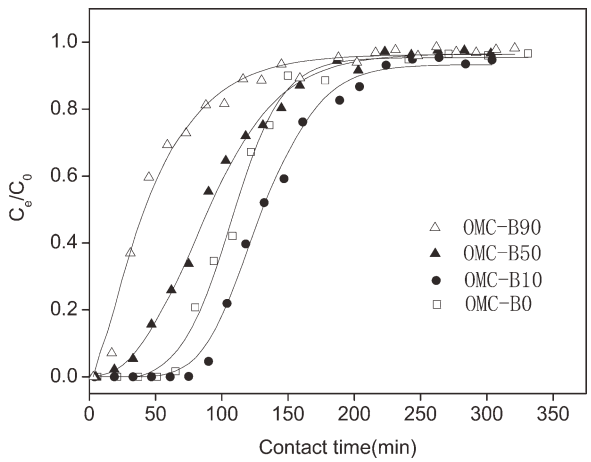

Figure 6 Breakthrough curves of naphthalene on the OMCs.

The isotherm parameters and correlation coefficients are tabulated in Table II. Higher determination coefficient (R^2) values showed that the Langmuir isotherms fit well with the adsorption data. The Langmuir isotherms could be used to estimate adsorption capacity of the OMCs. The equilibrium constant is associated with the affinity of the adsorption sites. It was clear from these results that the surface structure of the OMCs did not significantly influence the adsorption capacity. So the equilibrium constant change did not achieve regularity with increasing temperature. Figure 7 shows that at certain temperatures (120, 150, and 180°C), the descending order of the equilibrium constant was OMC-B10 > OMC-B0 > OMC-B50 > OMC-B90, and the order was same for the Q_0 value (Table II). Combined with the previous analytical results, this demonstrated that the rules were relevant to the mesopore size distribution. Also, both the adsorption rate and desorption rate of naphthalene on the OMCs increased when the mesopore size was larger. Therefore, the mesoporous structure with appropriate pore size was one of the key factors in enhancing the naphthalene adsorption capacity of the OMCs.

Adsorption kinetics of naphthalene on the OMCs

The Langmuir adsorption rate equation can be expressed by the following equation:

$$\frac{d\theta}{dt} = k(1 - \theta) \tag{3}$$

where θ is the surface coverage ($0 \leq \theta \leq 1$) and k is the rate constant (min^{-1}).

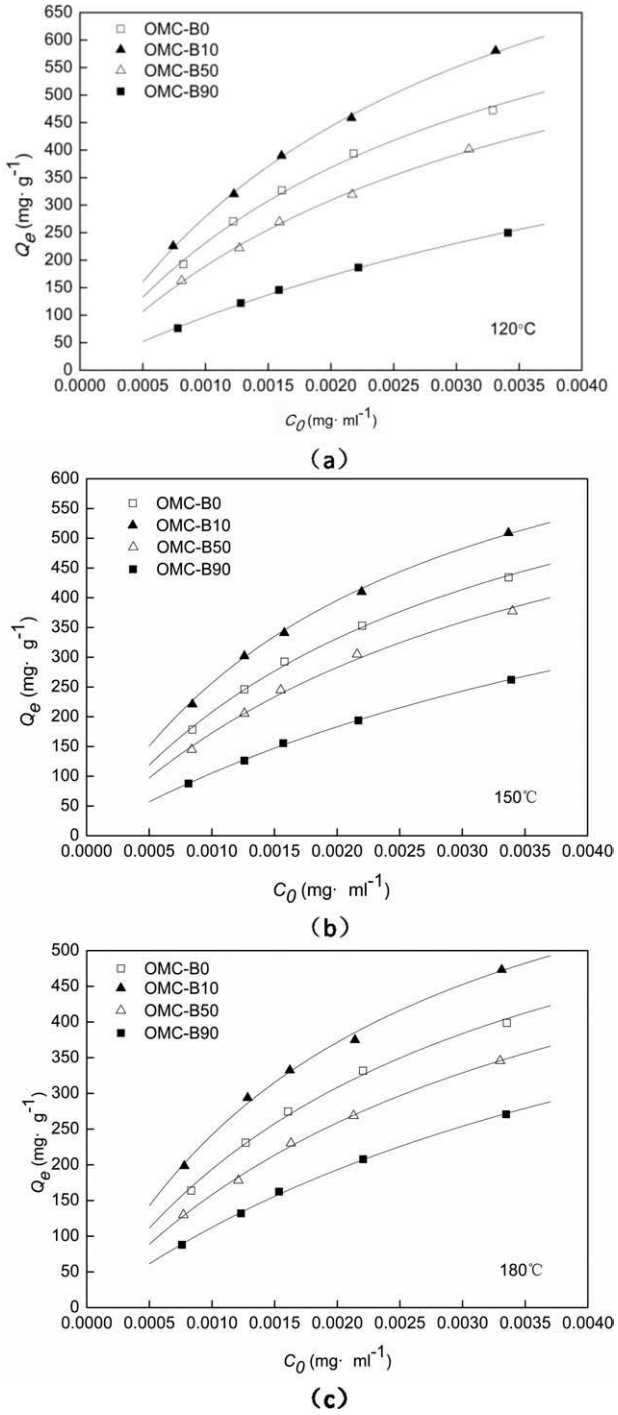

Figure 7 Adsorption and Langmuir isotherms for naphthalene on OMCs at (a) 120, (b) 150, and (c) 180°C.

Multiplied by Q_e on both sides of eq. (3), the linearized form of eq. (3) is written as follows:

$$\ln(Q_e - Q_t) = -kt + C \quad (4)$$

where Q_t is the adsorption capacity at time t (mg/g).

Figure 8 shows the fitting plots of $\ln(Q_e - Q_t)$ versus t at 150°C on the basis of pseudo-first-order kinetics, and the parameters of the Langmuir adsorption kinetics model of naphthalene on the OMCs are listed in Table III. It was obvious that the plot of $\ln(Q_e - Q_t)$ versus t at 150°C had a linear relationship. R^2 was higher than 0.98; this indicated that the adsorption of naphthalene onto the mesoporous carbons fit the pseudo-first-order rate equation. The descending order of the adsorption rate was OMC-B90 > OMC-B50 > OMC-B0 > OMC-B10, and this order was the same for the mesopore volume of the OMCs shown in Table I. It appears from these data that the adsorption rate followed the mesopore volume. However, the order was opposite with the naphthalene adsorption capacity and mesopore volume between 2 and 3.5 nm. This indicated that the mesopore volume between 2 and 3.5 nm and the pore sizes of the OMCs are crucial to the adsorption capacity and those OMCs with pore sizes of 2–3.5 nm were much more favorable in terms of the adsorption capacity.

TABLE II
Parameters of the Langmuir Model for Naphthalene Adsorption on the OMCs

Temperature (°C)	Sample	Langmuir isotherm		
		Q_0 (mg/g)	b (mL/mg)	R^2
120	OMC-B0	900.9	345.67	0.99165
	OMC-B10	1071.1	348.20	0.98991
	OMC-B50	840.3	290.85	0.99493
	OMC-B90	735.3	152.46	0.9912
150	OMC-B0	819.7	340.5	0.99452
	OMC-B10	943.4	360.00	0.99107
	OMC-B50	781.25	283.80	0.99027
	OMC-B90	704.2	175.81	0.99628
180	OMC-B0	769.2	339.80	0.99372
	OMC-B10	854.7	390.74	0.99322
	OMC-B50	714.3	284.40	0.99663
	OMC-B90	684.9	196.46	0.99533

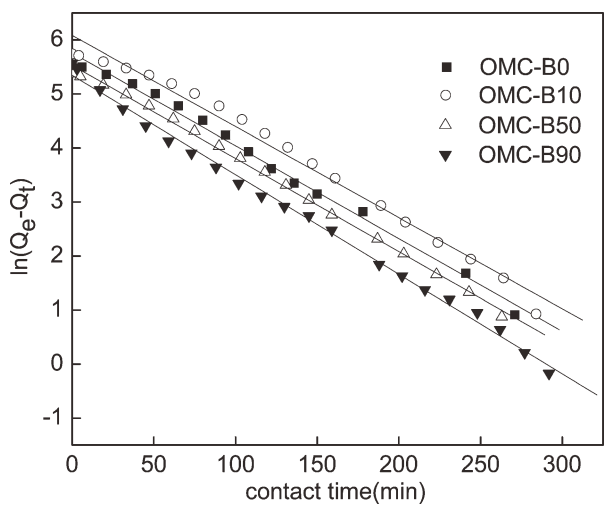

Figure 8 Adsorption kinetic curves of naphthalene on the OMCs.

TABLE III
Parameters of Langmuir Adsorption Kinetics Model of Naphthalene on the OMCs

Adsorbent	Langmuir equation	R^2	K
OMC-B0	$\ln(Q_e - Q_t) = -0.01719t + 5.76242$	0.99295	0.01719
OMC-B10	$\ln(Q_e - Q_t) = -0.01687t + 6.08425$	0.98583	0.01687
OMC-B50	$\ln(Q_e - Q_t) = -0.01725t + 5.53235$	0.99760	0.01725
OMC-B90	$\ln(Q_e - Q_t) = -0.01844t + 5.35$	0.99778	0.01844

CONCLUSIONS

In this study, OMCs were synthesized, and the naphthalene adsorption performance on the OMCs was investigated. Some conclusions were drawn, as follows:

1. OMCs with an ordered 2D hexagonal mesostructure were prepared successfully by a soft-template method with boric acid as a pore regulator. The mesopore sizes of the OMCs prepared were tunable and followed the boric acid content, and OMC-B90 had the largest mesopore size of 4.7 nm.
2. The dynamic adsorption of naphthalene on the OMCs showed that the maximum adsorption amount was above 303 mg/g. There was a close correlation between the adsorption capacity and the mesopore volume between 2 and 3.5 nm of the OMCs. Additionally, the mesopore size and distribution were critical to the adsorption capacity, and OMCs with mesopore sizes of 2–3.5 nm were much more favorable in terms of the adsorption capacity.
3. The adsorption isotherms of naphthalene on the OMCs matched the Langmuir adsorption isotherm well, and theoretical studies indicated that the adsorption kinetics of naphthalene on the OMCs accounted well for the use of the Langmuir adsorption kinetics equation.

References

1. International Agency for Research on Cancer. Polynuclear Aromatic Compounds, Part 1: Chemical, Environmental, and Experimental Data; IARC Monographs on the Evaluation of Carcinogenic Risk of Chemicals to Humans; World Health Organization: Lyon, France, 1983.
2. Evaluation and Estimation of Potential Carcinogenic Risks of PAH: Carcinogen Assessment Group; U.S. Environmental Protection Agency: Washington, DC, 1985.
3. Muller, P.; Leece, B.; Raha, D. Scientific Criteria Document for Multimedia environmental standards development: Polycyclic aromatic hydrocarbons (PAH). Part 1. Hazard Identification and Dose–Response Assessment; Ministry of the Environment and Energy: Ottawa, Ontario, 1997.
4. Sloss, L. L.; Gardner, C. A. Sampling and Analysis of Trace Emissions from Coal-Fired Power Stations; International Energy Agency Coal Research (IEACR): London, 1995.
5. Mastral, A. M.; Callén, M. S.; Murillo, R.; García, T. Environ Sci Technol 1999, 33, 3177.
6. Lee, W. M.; Tong, H. C.; Yeh, S. Y. Environ Sci Health A 1993, 28, 563.
7. Gerde, P.; Scholander, P. Adsorption of Polycyclic Aromatic Hydrocarbons on to Asbestos and Man-Made Mineral Fibres in the Gas Phase; IARC Scientific: Lyon, France, 1989; p 140.
8. Hart, K. M.; Pankow, J. F. Environ Sci Technol 1994, 28, 655.
9. Dachs, J.; Eisenreich, S. J. Environ Sci Technol 2000, 34, 3690.
10. Mastral, A. M.; Garciäa, T.; Calleän, M. S.; Navarro, M. V.; Galbaän, J. Environ Sci Technol 2001, 35, 2395.
11. Avom, J.; Mbadcam, J. K.; Noubactep, C.; Germain, P. Carbon 1997, 35, 365.
12. Xu, R. R.; Pang, W. Q.; Yu, J. H. Molecular Sieves and Porous Material Chemistry; Science Press: Beijing, 2004.
13. Xu, D. P.; Yoon, S. H.; Mochida, I.; Qiao, W. M.; Wang, Y. G.; Ling, L. C. Micropor Mesopor Mater 2008, 115, 461.
14. Yan, C. X.; Wang, C. Q.; Yao, J. F.; Zhang, L. X.; Liu, X. Q. Colloids Surf A 2009, 333, 115.
15. Zhao, D. Y.; Feng, J. L.; Huo, Q. S.; Melosh, N.; Fredrickson, G. H.; Chmelka, B. F.; Stucky, G. D. Science 1998, 279, 548.
16. Ryoo, R.; Joo, S. H.; Jun, S. J Phys Chem B 1999, 103, 7743.
17. Lee, H. I.; Kim, J. H.; You, D. J.; Lee, E. J.; Seung, D. Y. Adv Mater 2008, 20, 757.
18. Joo, S. H.; Lee, H. I.; You, D. J. Carbon 2008, 46, 2034.
19. Lee, J.; Yoon, S.; Hyeon, T.; Oh, S. M.; Kim, K. B. Chem Commun 1999, 2177.
20. Davis, M. E. Nature 2002, 417, 813.
21. Chai, G.; Yoon, S.; Yu, J.; Choi, J.; Sung, Y. J Phys Chem B 2004, 108, 7074.
22. Han, S.; Sohn, K.; Hyeon, T. Chem Mater 2000, 12, 3337.
23. Tanthapanichakoon, W.; Ariyadejwanich, P.; Japthong, P.; Nakagawa, K.; Mukai, S. R.; Tamon, H. Water Res 2005, 39, 1347.
24. Guo, Z.; Zhu, G. S.; Qiu, S. L. Carbon 2005, 43, 2344.
25. Yuan, X.; Xing, W.; Zhuo, S. P. J Colloid Interface Sci 2008, 322, 558.
26. Asouhidou, D. D.; Triantafyllidis, K. S.; Lazaridis, N. K. Micropor Mesopor Mater 2009, 117, 257.
27. Delage, F.; Pré, P.; Le, C. P. Environ Sci Technol 2000, 34, 4816.
28. Mastral, A. M.; García, T.; Callén, M. S.; Navarro, M. V.; Galbán, J. Environ Sci Technol 2001, 35, 2395.
29. Brosillon, S.; Manero, M. H.; Foussard, J. N. Environ Sci Technol 2001, 35, 3571.
30. Murillo, R.; García, T.; Aylón, E.; Callén, M. S.; Navarro, M. V.; López, J. M.; Mastral, A. M. Carbon 2009, 42, 2017.
31. Meng, Y.; Gu, D.; Zhang, F. Q.; Shi, Y. F.; Yang, H. F. Angew Chem Int Ed 2005, 44, 7053.
32. Meng, Y.; Gu, D.; Zhang, F. Q.; Shi, Y. F.; Cheng, L. Chem Mater 2006, 18, 4447.
33. Lin, H. P.; Chang, C. Y.; Tang, C. Y.; Lin, C. Y. Micropor Mesopor Mater 2006, 93, 344.
34. Kuo, S. W.; Lin, C. L.; Chang, F. C. Macromolecules 2002, 35, 278.
35. Ravikovitch, P. I.; Neimark, A. V. Colloids Surf A 2001, 11, 187.
36. Yang, C. M.; Zibrowius, B.; Schmidt, W.; Schuth, F. Chem Mater 2003, 15, 3739.
37. Trick, K. A.; Saliba, T. E. Carbon 1995, 33, 1509.
38. Kim, J.; Lee, J.; Hyeon, T. Carbon 2004, 42, 2711.
39. Liu, R. L.; Shi, Y. F.; Wan, Y. J. Am Chem Soc 2006, 128, 11652.
40. Kruk, M.; Jaroniec, M.; Ko, C. H.; Ryoo, R. Chem Mater 2000, 12, 1961.
41. Febrianto, J.; Kosasih, A. N.; Sunarso, J. J Hazard Mater 2009, 162, 616.
42. Sangi, M. R.; Shahmoradi, A.; Zolgharnein, J.; Azimi, G. H.; Ghorbandoost, M. J Hazard Mater 2008, 155, 513.